

C. R. Acad. Sci. Paris, t. 2, Série IV, p. 1–17, 2001
Atomes, molécules/*Atoms, molecules*

CONDENSATS DE BOSE–EINSTEIN ET LASERS À ATOMES *BOSE–EINSTEIN CONDENSATES AND ATOM LASERS*

Coherent manipulation of atoms with standing light waves

Subhadeep GUPTA, Aaron E. LEANHARDT, Alexander D. CRONIN, David E. PRITCHARD

Department of Physics and Research Laboratory of Electronics, Massachusetts Institute of Technology,
Cambridge, MA 02139, USA
E-mail: dpritch@mit.edu

(Reçu le 12 janvier 2001, accepté le 13 mars 2001)

Abstract. Coherent manipulation of atomic momentum states is the primary goal of atom optics, and the standing light wave with its associated stimulated light forces is the primary method of achieving this goal. A description of the standing wave as two counter-propagating beams of photons leads to a natural explanation of Bragg scattering. In contrast, Kapitza–Dirac scattering, atom lithography, and the matter-wave Talbot effect are more naturally treated by considering the standing light wave as a stationary field which acts as a periodic potential for the passing atoms or atomic waves. Selected experimental and theoretical results in the various qualitatively different regimes of the standing wave–atom interaction are reviewed, with special attention given to the physical differences underlying the various behaviors and the theoretical approximations used to treat them. © 2001 Académie des sciences/Éditions scientifiques et médicales Elsevier SAS

atom optics / matter wave diffraction / Bragg scattering / Kapitza–Dirac scattering / atom lithography / Talbot effect

Manipulation cohérente d'atomes avec des ondes lumineuses stationnaires

Résumé. *La manipulation cohérente d'états d'impulsion définie est le but premier de l'optique atomique, et l'onde stationnaire lumineuse avec les forces radiatives stimulées qui lui sont associées, est la méthode première pour y parvenir. Une description de l'onde stationnaire en termes de deux faisceaux de photons contre-propageants, conduit à une explication naturelle de la diffraction de Bragg. Au contraire, la déflexion de type Kapitza–Dirac, la lithographie atomique, l'effet Talbot des ondes de matière, se décrivent plus naturellement en considérant l'onde lumineuse stationnaire comme un champ qui joue le rôle d'un potentiel périodique pour les atomes (ou les ondes de matière) qui le traversent. On présente quelques résultats expérimentaux et théoriques dans les divers régimes de l'interaction atome–onde stationnaire, en soulignant les différences physiques qui sous-tendent les divers comportements et les approximations théoriques permettant de les traiter.* © 2001 Académie des sciences/Éditions scientifiques et médicales Elsevier SAS

optiques atomiques / diffraction matière onde / déflexion de Bragg / déflexion Kapitza–Dirac / lithographie atomique / l'effet Talbot

Note présentée par Guy LAVAL.

1. Introduction

The foremost goal of atom optics is to manipulate atomic waves coherently. This can facilitate the creation of atom interferometers, atom microscopes, high resolution atom lithography, and the incorporation of coherent atomic center-of-mass manipulation within an environment where internal atomic coherences are also being exploited. With the development of tunable lasers, the chief tool for such coherent manipulation has become a standing wave of near-resonant radiation.

In many respects, the interaction of an atom with a standing light wave is richer in several ways than the more familiar topic of light-atom interactions within a traveling light wave. Part of this richness reflects the two ways in which a standing wave can be considered, either as two counter-propagating traveling waves or as a single, stationary standing wave. The standing wave-atom interaction is capable of transferring momentum in well-determined quantities, coherently splitting atomic wavepackets, and generating forces much larger than possible with spontaneously scattered light. Not surprisingly, this interaction has many distinct facets that only appear in different regimes of the interaction parameters (intensity, detuning, and pulse duration) and atomic parameters (mass, initial momentum with respect to the standing wave, and excited state natural lifetime). This paper is a review of the major regimes of this rich physics that have been explored experimentally and theoretically over the last two decades.

The underlying physics of atom optics was developed by the pioneers of quantum mechanics. Their starting point, the question of whether light is a particle or a wave, is embodied in the duality just mentioned as to whether a standing wave is better considered as two counter-propagating beams of photons or a stationary electromagnetic field. As we have recently discussed the history of atom optics in some generality [1], we shall discuss here only the first proposal for coherent matter wave manipulation by Kapitza and Dirac in 1933 [2]. They proposed that stimulated Compton scattering could be used to reflect an electron beam from a standing light wave. In general, a stimulated scattering process transfers a photon from one traveling light wave into another with the difference in momentum of the two photons being imparted onto the particle. The stimulated Compton scattering process proposed by Kapitza and Dirac has a very small cross section, given by the classical electron radius squared, $\sigma_{\text{Compton}} = \frac{8\pi}{3}(e^2/m_e c^2)^2 \approx 6 \cdot 10^{-25} \text{ cm}^2$. With the experimentally available laser intensities, the small cross section makes this scattering process challenging to observe and separate from background processes [3-6]. However, if the stimulated light scattering process occurs with atoms instead of electrons, then the cross section is tremendously larger; for near-resonant light it is $\sigma_{\text{atom}} = \frac{3}{2\pi}\lambda_{\text{photon}}^2 \approx 1 \cdot 10^{-9} \text{ cm}^2$, which is large enough to be observed at modest laser intensities. This large cross section, together with the ready availability of tunable lasers, has allowed stimulated scattering to become the primary tool for the coherent manipulation of atoms. An important feature of stimulated scattering processes is that they are highly dependent on the species of atom and even its internal and external (momentum) states as we now discuss.

2. Bragg scattering

We begin with the Bragg scattering of atoms from a standing wave light grating. Although it can be difficult to realize the physical conditions that assure its occurrence, Bragg scattering is the simplest example of coherent momentum transfer to atoms by light. Consider a standing wave light grating formed by two counter-propagating plane waves (traveling parallel to the z -axis) of equal amplitude, E_0 , wavevector, k , frequency, ω , polarization vector, \hat{e} , and temporal envelope function, $f(t)$:

$$\vec{E}(z, t) = E_0 f(t) \sin(kz - \omega t) \hat{e} + E_0 f(t) \sin(kz + \omega t) \hat{e} \quad (1)$$

$$= 2E_0 f(t) \sin(kz) \cos(\omega t) \hat{e} \quad (2)$$

We would like to work with momentum states as our basis, thus it is easiest to consider the description of the electric field driving the transitions in terms of two counter-propagating traveling waves of definite momentum (equation (1)), as opposed to the single standing wave they jointly form (equation (2)).

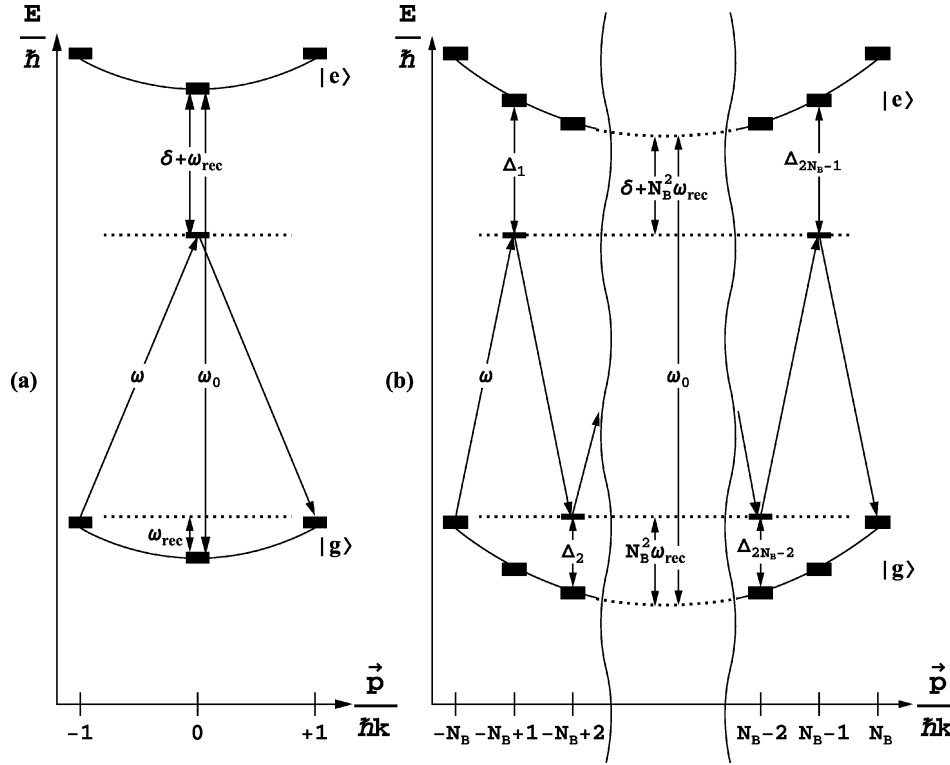


Figure 1. (a) First and (b) N_B -th-order Bragg transition diagram. The atomic kinetic energy lies on the parabola $N^2\hbar\omega_{rec}$, $N = 0, \pm 1, \pm 2, \dots$ where the associated atomic momentum is given by $N\hbar k$.

Momentum is transferred by paired stimulated absorption and emission processes, resulting in a transfer of photons between the traveling waves. An N_B -th-order diffraction process transfers N_B photons from one traveling wave to the counter-propagating traveling wave and changes the atomic momentum by $2N_B\hbar k$. Furthermore, atomic population is transferred only between $|g, -N_B\hbar k\rangle$ and $|g, +N_B\hbar k\rangle$, where $|g(e), \pm N\hbar k\rangle$ denotes a two-level atom in its ground (excited) state with momentum $\pm N\hbar k$ parallel to the standing wave axis. The excited state remains nominally unpopulated so long as the temporal envelope function, $f(t)$, does not have strong frequency components near the laser detuning, $\delta = \omega - \omega_0$, where ω_0 is the unperturbed frequency of the atomic transition. Furthermore, for a given initial state ($|g, -N_B\hbar k\rangle$) the uniqueness of the final state ($|g, +N_B\hbar k\rangle$) comes about because of the fundamental assumption that makes Bragg scattering so simple to describe; the uncertainty in the photon energy driving the transitions is small compared to the energy separation between neighboring momentum states. A quantitative discussion of the validity of this assumption will be given later.

We now calculate the probability, $P_1^B(\tau)$, of the first-order ($N_B = 1$) Bragg process taking an atom from $|g, -\hbar k\rangle$ to $|g, +\hbar k\rangle$ when the atoms interact with a constant light intensity for a time τ (i.e. in equations (1) and (2) $f(t)$ is a square wave of unit amplitude and duration τ). The transition is depicted in *figure 1a*. In the electric dipole approximation, the interaction Hamiltonian is $\mathcal{H}_{int}(t) = -\vec{\mu} \cdot \vec{E}(t)$. By momentum conservation, only the plane wave traveling in the $\pm \hat{z}$ direction couples the $|e, 0\rangle \leftrightarrow |g, \mp 1\rangle$ transitions. By using this argument, we are effectively viewing the electric field as a quantum mechanical operator. Expanding the sinusoidal variation of the electric field in terms of complex exponentials and treating the spatially dependent complex exponential terms as quantum mechanical momentum translation operators

S. Gupta et al.

BOSE-EINSTEIN CONDENSATES AND ATOM LASERS

($e^{\pm ik\hat{z}}|g(e), n\hbar k\rangle = |g(e), (n \pm 1)\hbar k\rangle$) yields the interaction Hamiltonian [9–11]:

$$\mathcal{H}_{\text{int}}(t) = -i e^{-i\omega t} \frac{\hbar\omega_R}{2} (|e, 0\rangle\langle g, -1| - |e, 0\rangle\langle g, +1|) + \text{h.c.} \quad (3)$$

where the depicted terms are responsible for absorption and the hermitian conjugate (h.c.) terms give rise to stimulated emission. The light–atom interaction is parameterized by the single-photon Rabi frequency,

$$\omega_R = \frac{\mu E_0}{\hbar} \quad (4)$$

where $\mu = \langle e|e\vec{r}|g\rangle \cdot \hat{e}$ is the electric dipole matrix element connecting the ground ($|g\rangle$) and excited ($|e\rangle$) states of the atom. Without loss of generality, we will take μ and hence ω_R to be positive, real-valued quantities. In formulating \mathcal{H}_{int} , we have neglected any frequency components associated with the sudden switch on of the fields and the finite duration of the light–atom interaction. The total Hamiltonian, $\mathcal{H}(t) = \mathcal{H}_0(t) + \mathcal{H}_{\text{int}}(t)$, follows simply by including the electronic and kinetic energy terms:

$$\mathcal{H}_0(t) = \hbar\omega_0|e, 0\rangle\langle e, 0| + \hbar\omega_{\text{rec}}(|g, -1\rangle\langle g, -1| + |g, +1\rangle\langle g, +1|) \quad (5)$$

where the single-photon recoil energy, E_{rec} , of an atom of mass m is given by:

$$E_{\text{rec}} = \hbar\omega_{\text{rec}} = \frac{\hbar^2 k^2}{2m} \quad (6)$$

Making the *ansatz* for the solution wavefunction as:

$$|\Psi(t)\rangle = c_{-1}(t) e^{-i\omega_{\text{rec}}t}|g, -1\rangle + c_0(t) e^{-i\omega_0 t}|e, 0\rangle + c_{+1}(t) e^{-i\omega_{\text{rec}}t}|g, +1\rangle \quad (7)$$

and substituting into the Schrödinger equation yields the three coupled first-order differential equations:

$$\dot{c}_{\pm 1}(t) = \mp \frac{\omega_R}{2} e^{i\Delta t} c_0(t) \quad (8)$$

$$\dot{c}_0(t) = \frac{\omega_R}{2} e^{-i\Delta t} (c_{+1}(t) - c_{-1}(t)) \quad (9)$$

where $\Delta = \delta + \omega_{\text{rec}}$. Differentiating equation (8) and substituting equation (9) into the result yields the two coupled second-order differential equations:

$$\ddot{c}_{\pm 1}(t) - i\Delta\dot{c}_{\pm 1}(t) + \frac{\omega_R^2}{4}(c_{\pm 1}(t) - c_{\mp 1}(t)) = 0 \quad (10)$$

With the initial conditions:

$$c_{-1}(0) = 1 \quad (11)$$

$$c_0(0) = 0 \implies \dot{c}_{\pm 1}(0) = 0 \quad (12)$$

$$c_{+1}(0) = 0 \quad (13)$$

and the assumption $\Delta^2 \gg \omega_R^2$, the solutions to equation (10) read:

$$c_{-1}(t) = e^{-\frac{1}{2}\omega_R^{(2)}t} \cos\left(\frac{\omega_R^{(2)}}{2}t\right) \quad (14)$$

$$c_{+1}(t) = i e^{-\frac{1}{2}\omega_R^{(2)}t} \sin\left(\frac{\omega_R^{(2)}}{2}t\right) \quad (15)$$

BOSE-EINSTEIN CONDENSATES AND ATOM LASERS

Coherent manipulation of atoms

where the two-photon Rabi frequency is:

$$\omega_R^{(2)} = \frac{\omega_R^2}{2\Delta} \rightarrow \frac{\omega_R^2}{2\delta}, \quad |\delta| \gg \omega_{\text{rec}} \quad (16)$$

with both transitions driven at equal single-photon Rabi frequencies, ω_R .

Substituting the solution of equation (14) or (15) into equation (8) yields an expression for the excited state amplitude:

$$c_0(t) = -i \frac{\omega_R}{2\Delta} e^{-i\Delta t} e^{-i\omega_R^{(2)} t} \quad (17)$$

This will be important in calculating the rate of spontaneous emission events later.

The solutions for $c_{-1}(t)$ and $c_{+1}(t)$ oscillate with the interaction duration, τ , yielding the result for the $|g, -\hbar k\rangle \rightarrow |g, +\hbar k\rangle$ transition probability:

$$P_1^B(\tau) = |c_{+1}(\tau)|^2 = \sin^2\left(\frac{\omega_R^{(2)}}{2} \tau\right) \quad (18)$$

Thus, the system oscillates between the two momentum states $|g, -\hbar k\rangle$ and $|g, +\hbar k\rangle$ in a manner analogous to the Rabi oscillation of atomic population between two resonantly coupled states. This solution with oscillatory probabilities for the two Bragg coupled states is known as the Pendellösung and has been observed for atoms [7], neutrons [12], and X-rays [13].

Viewing Bragg scattering as a two-photon transition from the initial ground state to the final ground state with opposite momentum illuminates the close connection with a Raman transition between two internal substates of the ground state manifold, each with its own external momentum state. The formalism describing the Raman transition is basically the same as that presented here, except the two transitions can be driven at different single-photon Rabi frequencies, ω_{R1} and ω_{R2} , so that the generic two-photon Rabi frequency is given by $\omega_R^{(2)} = \omega_{R1}\omega_{R2}/2\Delta$, where Δ is the detuning from the intermediate state.

An N_B -th-order Bragg process (similar to a $2N_B$ -photon Raman process) is a coherent succession of N_B two-photon transitions with $2N_B - 1$ intermediate states of the form

$$|e, (-N_B + 1)\hbar k\rangle, \quad |g, (-N_B + 2)\hbar k\rangle, \quad \dots, \quad |g, (N_B - 2)\hbar k\rangle, \quad |e, (N_B - 1)\hbar k\rangle$$

Such a process is characterized by a $2N_B$ -photon Rabi frequency given by [14]:

$$\omega_R^{(2N_B)} = \frac{[\omega_R]^{2N_B}}{2^{2N_B-1} \Delta_1 \Delta_2 \dots \Delta_{2N_B-1}} \quad (19)$$

where Δ_n is the detuning from the n th intermediate state. *Figure 1b* shows what this process would look like for an N_B -th-order Bragg transition where the intermediate state detunings are given by:

$$\Delta_n = \begin{cases} \delta + (2N_B n - n^2)\omega_{\text{rec}}, & n \text{ odd} \\ (2N_B n - n^2)\omega_{\text{rec}}, & n \text{ even} \end{cases} \quad (20)$$

Substituting these detunings into equation (19) yields the N_B -th-order Bragg transition $2N_B$ -photon Rabi frequency, $\omega_R^{(2N_B)}$ [14]:

$$\omega_R^{(2N_B)} = \frac{[\omega_R]^{2N_B}}{2^{4N_B-3} [(N_B - 1)!]^2 \delta^{N_B} \omega_{\text{rec}}^{N_B-1}} \quad (21)$$

where we have assumed $|\delta| \gg N_B^2 \omega_{\text{rec}}$.

To ensure that the system truly undergoes Bragg scattering, and validate the assumption that only states of equal kinetic energy and opposite momentum are coupled, the overall exposure time, τ , of the atoms to the fields must be limited both from below and above.

The lower bound on τ is necessary to resolve the final momentum state ($|g, N_B \hbar k\rangle$) from neighboring momentum states ($|g, (N_B \pm 2) \hbar k\rangle$) two photon recoil momenta away. This bound also prohibits resonant transitions from the initial momentum state ($|g, -N_B \hbar k\rangle$) to its neighboring momentum states ($|g, (-N_B \pm 2) \hbar k\rangle$) two photon recoil momenta away. For first order Bragg scattering processes ($N_B = 1$) the initial and final state are only separated by two photon recoil momenta, thus the nearest lying momentum states that may be mistakenly populated are $|g, \pm 3 \hbar k\rangle$. Avoiding population transfer into these states requires $\tau \gg \pi/4\omega_{\text{rec}}$. For all higher-order ($N_B > 1$) Bragg scattering processes, the nearest momentum states are $|g, \pm(N_B - 2) \hbar k\rangle$, which limits the interaction time to:

$$\tau \gg \frac{\pi}{2(N_B - 1)\omega_{\text{rec}}} \quad (22)$$

which for $N_B \gg 1$ reduces to:

$$\tau \gg \frac{\pi}{2N_B\omega_{\text{rec}}} \quad (23)$$

The upper bound on the interaction duration is necessary to avoid spontaneous emission. The interaction duration must be short enough so that the expected number, N_s , of spontaneous emission events per atom during the time τ is negligible. N_s is simply given by the product of the excited state fraction (equation (17)) and the probability of spontaneous decay given that the atom is in the excited state:

$$N_s = |c_0(t)|^2 \Gamma \tau = \frac{\omega_R^2}{4\Delta^2} \Gamma \tau \quad (24)$$

where Γ is the natural decay rate of the excited state. Avoiding spontaneous emission ($N_s \ll 1$) while still having a significant probability for transitions ($\omega_R^{(2N_B)} \tau \simeq \pi$) forces one to work in the regime where $\Delta^2 \gg \omega_R^2$, which we assumed earlier but now see is a practical requirement to avoid spontaneous emission and maintain coherence.

Bragg scattering of atoms from a standing light wave was first observed at MIT in 1988 [7]. A supersonic atomic beam was diffracted from a standing wave of near-resonant laser light. The angle between the atomic beam (of thermal wavelength λ_{dB}) and the light grating (of periodicity $\lambda_L/2$) was tuned to the appropriate Bragg angle, θ_B , where:

$$\lambda_{\text{dB}} = \lambda_L \sin(\theta_B) \quad (25)$$

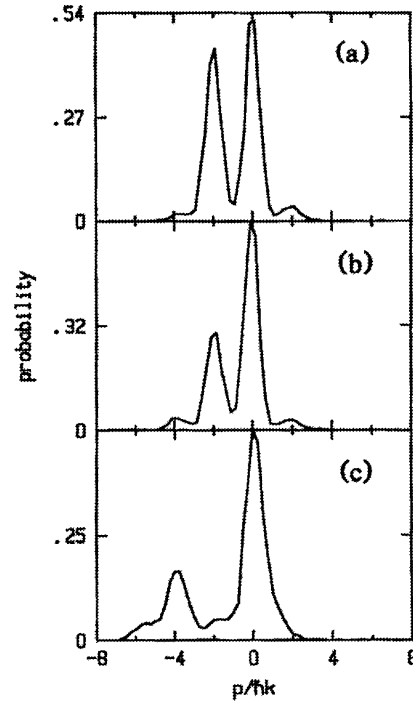
and population transfer corresponding to both first and second order Bragg scattering was observed (figure 2). The experiment required a sub-recoil transverse momentum spread of the atomic beam in order to resolve the different momentum states in the far field and limit the final state to only one diffracted order. The Pendellösung was observed as an oscillation in population transfer as a function of standing wave intensity, $I \propto \omega_R^{(2)}$, for a fixed interaction time, τ .

Atomic beam diffraction from an optical standing wave is a continuous-wave (CW) experiment in which the selectivity needed for the Bragg process is imposed by good angular resolution of the particle beam and a high degree of parallelism between the light crystal planes. This ensures that of the various final Bragg orders allowed by momentum conservation, only one conserves energy (energy conservation is exact in a CW experiment). For atoms scattering from a light crystal, parallelism of the crystal planes requires highly parallel photon momentum that implies a minimum width of the standing wave (the diffraction limit for the collimated photons). The transit time, τ , of the atoms across this width then exceeds the lower bound given in equation (22).

BOSE-EINSTEIN CONDENSATES AND ATOM LASERS

Coherent manipulation of atoms

Figure 2. Bragg scattering of an atomic beam from an optical standing wave. First-order Bragg scattering at (a) $\omega_R^{(2)}\tau = 3.8$ and (b) $\omega_R^{(2)}\tau = 6.4$ (the oscillatory Pendellösung returns atoms to their original state). (c) Second-order Bragg scattering. Figure from [7].



The excellent collimation required of the atomic beam to ensure resolution of the Bragg scattered atoms reduces the intensity of the source by many orders of magnitude. A Bose–Einstein Condensate (BEC) is an attractive alternative source of atoms because its momentum spread is typically an order of magnitude below a single-photon recoil momentum. To Bragg diffract atoms initially in a stationary BEC, it is easier to move the light crystal than to accelerate the condensate. This is done by simply frequency shifting one of the traveling waves so that the resultant standing wave formed by its interference with the unshifted traveling wave moves with the proper velocity ($N_B\hbar k/m$) relative to the stationary atoms to impart the necessary momentum. The Bragg scattered atoms will then have momentum $2N_B\hbar k$ in the laboratory frame. The resonance condition thus becomes a condition on relative detuning, δ_{N_B} , between the two laser beams forming the diffraction grating. For N_B -th-order Bragg diffraction, the relative detuning is given by:

$$\delta_{N_B} = \frac{2N_B\hbar k^2}{m} = 4N_B\omega_{rec} \tag{26}$$

The first demonstration of Bragg scattering in a BEC was at NIST in 1999 [15]. They used Bragg scattering mainly as a tool to manipulate the momentum of the BEC, observing up to sixth-order processes. At MIT the interaction time was lengthened (to ≈ 100 times the lower bound of equation (22) for first-order Bragg scattering), creating a new type of spectroscopy called Bragg spectroscopy. This was used to observe the momentum distribution of a BEC in a magnetic trap [8]. The width of the Bragg resonance curve (figure 3) was primarily due to a 2 kHz Doppler-broadening that yielded the momentum distribution of the condensate. The spread in the corresponding velocity distribution was very small (≈ 0.5 mm/s), even smaller than allowed by the Heisenberg uncertainty limit for a particle confined in the ground state of a harmonic trap. This reflects the increase in size of the condensate due to the mean-field repulsion (^{23}Na , used in the MIT experiment, has a positive scattering length). The distribution was Heisenberg uncertainty limited at the observed size of the BEC, establishing for the first time that the coherence length of the

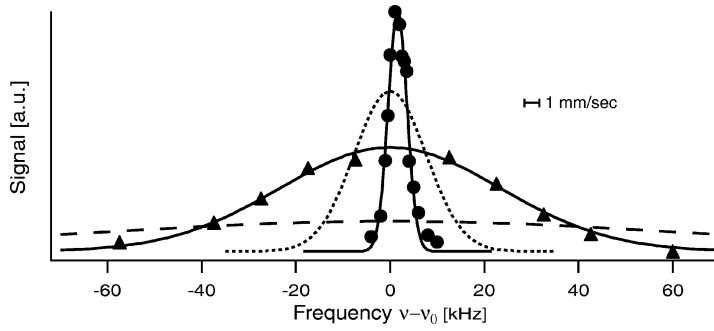


Figure 3. Resonances in Bragg scattering rate vs. grating speed for a trapped condensate (circles, height scaled by 0.2) and of a released condensate (triangles). $\nu_0 = 2\omega_{\text{rec}}/\pi$ is the resonance frequency of a non-interacting condensate. For comparison, the momentum distributions of the ground state of the trapping potential (dotted curve, height scaled by 0.5) and of a $1 \mu\text{K}$ thermal cloud (dashed curve) are indicated. Figure adapted from [8].

condensate was equal to its size. In addition, the narrow Bragg resonance was shifted by the repulsive interactions within the condensate, resulting in a spectroscopic measurement of the mean-field energy.

3. Kapitza–Dirac scattering

In 1933, Kapitza and Dirac predicted that an electron beam incident onto a properly orientated standing light wave would undergo stimulated Compton scattering and be reflected [2]. Since then, scattering that can be properly described by neglecting particle motion over the duration of the interaction (the Raman–Nath approximation) has become known as Kapitza–Dirac scattering. Atoms may also undergo such scattering from a standing light wave, and as described in the introduction, the cross-section for this process can be tremendously enhanced by tuning the light near an atomic transition.

To restrict the atomic motion during the interaction time to distances small compared to the characteristic dimensions of the interaction potential requires short interaction times. Mathematically, this regime can be treated by neglecting the atomic kinetic energy term in the Hamiltonian (the Raman–Nath approximation). This is equivalent to the eikonal (thin-lens) approximation for scattering (optics). For a standing wave interaction, this approximation is well satisfied if the atomic motion during the interaction time is small compared to the wavelength of the illuminating radiation. As a result, Kapitza–Dirac scattering is limited (relative to Bragg scattering) to short interaction times, τ , generally much smaller than the inverse recoil frequency ($\tau \ll 1/\omega_{\text{rec}}$). To observe appreciable population transfer at such short times, large intensities are needed. Since Kapitza–Dirac scattering is a coherent process, the interaction time must also be short enough to make spontaneous emission negligible. Thus the constraint $N_s \ll 1$ (equation (24)) holds in this regime as well, where N_s is the expected number of spontaneous emission events per atom during the time τ . We shall discuss the regime where this approximation is violated in the subsequent section on atom lithography.

The standing wave interaction may be treated by considering the standing wave (AC Stark shift) potential resulting from the applied fields given in equations (1) and (2):

$$U(z, t) = \frac{\hbar\omega_R^2}{\delta} f^2(t) \sin^2(kz) \quad (27)$$

where we have assumed $\delta^2 \gg I^2/4$.

The quickest route to the momentum distribution of the diffracted atoms in the Kapitza–Dirac regime is to use the eikonal approximation for treating the scattering of the incident atomic waves after passing through the AC Stark shift potential of the standing wave. Given the initial atomic wavefunction, $|\Psi_0\rangle$, the

atomic wavefunction immediately after the interaction is given by:

$$|\Psi\rangle = |\Psi_0\rangle e^{-\frac{i}{\hbar} \int dt' U(z, t')} = |\Psi_0\rangle e^{-\frac{i}{2\delta} \omega_R^2 \tau} e^{\frac{i}{2\delta} \omega_R^2 \tau \cos(2kz)} \quad (28)$$

where $\tau = \int dt' f^2(t')$ and the integral is over the interaction duration. With the use of the identity for Bessel functions of the first kind, $e^{i\alpha \cos(\beta)} = \sum_{n=-\infty}^{\infty} i^n J_n(\alpha) e^{in\beta}$, the atomic wavefunction can be written as:

$$|\Psi\rangle = |\Psi_0\rangle e^{-\frac{i}{2\delta} \omega_R^2 \tau} \sum_{n=-\infty}^{\infty} i^n J_n\left(\frac{\omega_R^2}{2\delta} \tau\right) e^{i2nkz} = e^{-\frac{i}{2\delta} \omega_R^2 \tau} \sum_{n=-\infty}^{\infty} i^n J_n\left(\frac{\omega_R^2}{2\delta} \tau\right) |g, 2n\hbar k\rangle \quad (29)$$

where the position space representation of the momentum states has been used ($|g, p\rangle = \mathcal{N} e^{ipz/\hbar}$, with \mathcal{N} an arbitrary normalization factor) and we have taken $|\Psi_0\rangle = |g, 0\rangle$.

It is now clear that states with $2N\hbar k$ of momentum are populated with probability [16,17]:

$$P_N = J_N^2(\theta), \quad N = 0, \pm 1, \pm 2, \dots, \quad \text{where} \quad (30)$$

$$\theta = \frac{\omega_R^2}{2\delta} \tau = \omega_R^{(2)} \tau \quad (31)$$

is the pulse area. This leads to a transverse rms momentum of the diffracted atoms that is linearly proportional to the pulse area [16]:

$$p_{\text{rms}} = \sum_{n=-\infty}^{\infty} (n\hbar k)^2 P_n = 2^{1/2} \theta \hbar k \quad (32)$$

Kapitza–Dirac diffraction of atoms was first observed at MIT in 1986 [16]. Diffraction of a well-collimated (sub-recoil) supersonic atomic beam was observed after passage through the tightly focused waist of a near-resonant standing wave. Significant diffraction into momentum states $|g, \pm 10\hbar k\rangle$ was observed [16] (figure 5). Even higher diffracted orders should be observable in the future using laser beams directed at small Bose–Einstein Condensates for somewhat longer times.

4. Atom lithography and the Talbot effect

Atom lithographic processes utilize atomic motion parallel to the standing wave axis during the light–atom interaction. Such appreciable motion is a violation of the Raman–Nath approximation that underlies Kapitza–Dirac scattering. A glance at figure 4 suggests a classical oscillation of atoms around the minima of the standing wave potential described by equation (27). This potential is approximately harmonic about its minima with curvature $\partial^2 U / \partial z^2 = 2\hbar\omega_R^2 k^2 / |\delta|$. Thus, an atom of mass m and transition wavevector k , with corresponding single-photon recoil frequency $\omega_{\text{rec}} = \hbar k^2 / 2m$ (equation (6)), will have an oscillation frequency:

$$\omega_{\text{osc}} = 2\omega_R \left(\frac{\omega_{\text{rec}}}{|\delta|} \right)^{1/2} \quad (33)$$

Thus the Kapitza–Dirac regime requires $\tau \ll \tau_{\text{osc}}/4$, where the oscillation period, τ_{osc} , is given by:

$$\tau_{\text{osc}} = \frac{\pi}{\omega_R} \left(\frac{|\delta|}{\omega_{\text{rec}}} \right)^{1/2} \quad (34)$$

The transition from the Kapitza–Dirac scattering regime to the classical oscillation regime ($\tau \geq \tau_{\text{osc}}/4$) has been studied with a BEC at NIST [17].

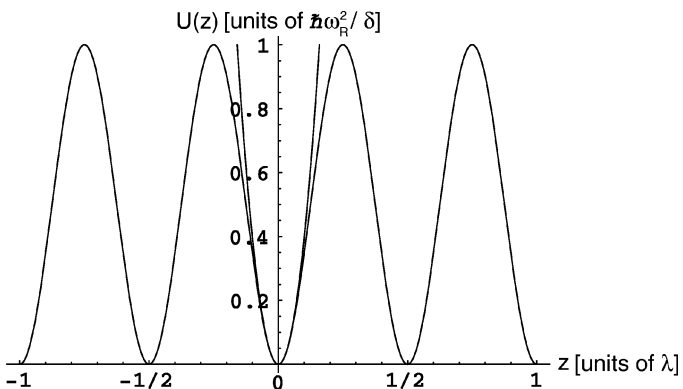


Figure 4. Standing wave light–atom interaction potential (in units of $\hbar\omega_R^2/\delta$) with the parabolic approximation near a minimum. The position axis is in units of the light wavelength, λ .

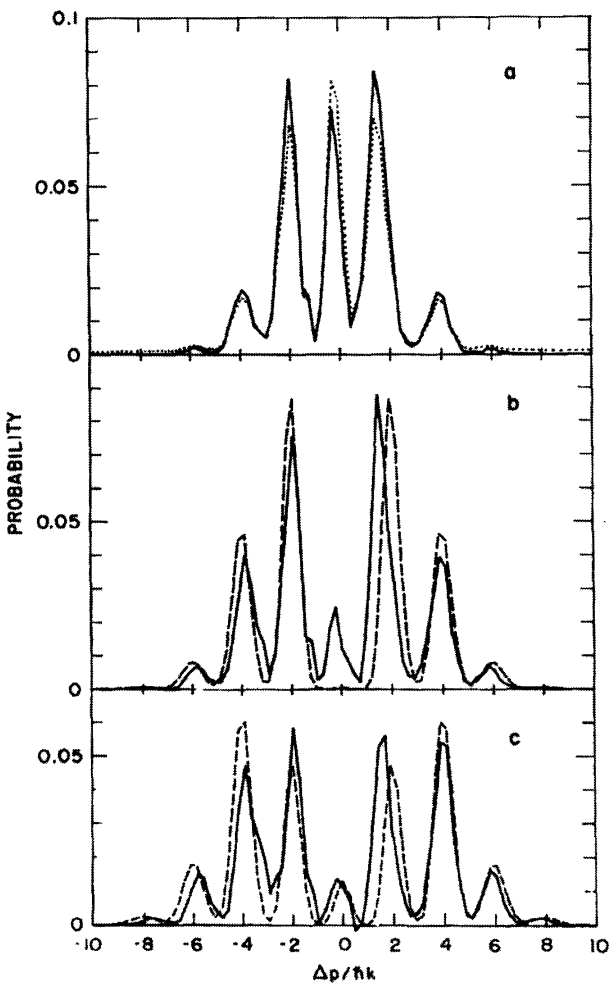


Figure 5. Kapitza–Dirac diffraction of an atomic beam from a standing wave light grating. (a) $\theta = 1.69$, a comparison of raw (dotted line) and corrected (solid line) data; (b) $\theta = 2.33$, a comparison of corrected data (solid line) and theory (dashed line); (c) $\theta = 2.84$, a comparison of corrected data (solid line) and theory (dashed line). Figure from [16] — see for details on data correction and theoretical curves.

The classical oscillation of atoms in the standing wave potential described above can produce spatially periodic bunches of atoms. Depositing these onto a surface constitutes atom lithography. Consider a well-collimated monochromatic atomic beam with longitudinal speed v normally incident on a standing wave light grating. In the harmonic approximation, if the light–atom interaction duration is $\tau_{\text{osc}}/4$ (or odd

multiples thereof), then all of the atoms will be found near the potential minima. If the field is maintained for less than this time, the atoms will be traveling toward the location of the minima and will reach a focus after exiting the standing wave region. Due to anharmonicities of the potential away from its minima, atoms starting higher up the edges of the standing wave potential wells will have longer periods. This degrades the quality of the focusing effects. While maintaining the fields for a duration $\tau = \tau_{\text{osc}}/4$ produces (periodically spaced) samples of atoms focused in position space, their transverse momentum distribution has a width of order $p_{\text{max}} = \omega_{\text{R}}(2\hbar m/\delta)^{1/2}$ (equation (41), to be discussed in Section 5) which limits the depth of focus. However, if the atoms encounter a substrate placed at the focus, then narrow stripes of atoms will be deposited forming a periodic grating with the same period as the standing wave. Such periodic structures have been realized with alkali atoms [19], aluminum [20], and chromium [21]. Chromium diffraction gratings fabricated by this method are used as a length standard for electron microscopes. As a natural generalization of this technique, a two-dimensional standing wave field can produce a regularly spaced two-dimensional array of small deposits [22].

Experimental work in atom lithography often operates in a regime where spontaneous emission readily occurs [19,21]. In contrast, most of the experimental work mentioned in this paper was accomplished with negligible spontaneous emission (due to the use of sufficiently large detunings). When spontaneous emission is prevalent, the average optical potential seen by the atoms is the pseudopotential [19,21,23,24]:

$$U(z, t) = \frac{1}{2}\hbar\delta \ln\left(1 + \frac{2\omega_{\text{R}}^2 f^2(t) \sin^2(kz)}{\delta^2 + (\Gamma/2)^2}\right) \quad (35)$$

not the AC Stark shift potential of equation (27). This pseudopotential is valid provided that the atoms have been exposed to the fields long enough to make a few spontaneous emissions [19]. In the limit of large detuning ($\delta^2 \gg \Gamma^2/4$), the pseudopotential given by equation (35) reduces to the optical potential given in equation (27).

In atom lithographic processes, such a short time passes between the atoms exiting the standing wave grating and landing on the substrate that the wave properties of the propagating atoms are unimportant, i.e. ray tracing using classical forces or indices of refraction works adequately to describe the atomic kinematics. However, as the atoms are allowed to propagate for longer times (farther into the near field (Fresnel) diffraction region) their wave nature becomes important. In particular, the self-imaging of the diffraction grating in the near field arises from the interference of waves scattered from neighboring potential wells. This effect was reported in 1836 by H.F. Talbot and now bears his name. He reported that in the paraxial region of the near field of a diffraction grating illuminated with optical waves, a perfect image of the grating was realized at integer multiples of what has become known as the Talbot length, L_{T} [25]. The first demonstration of the Talbot effect with atoms was done at MIT in 1995 and is shown in figure 6 [18]. Images of the grating also arise at lengths that are a rational fraction of the Talbot length, but with altered phase and periodicity. This fractional Talbot effect has been used in electromagnetic wave [26–28] and atom [29] lithography to produce gratings of finer periodicity than the original in a process known as *spatial-period division*.

To derive the Talbot length for atom optics we consider an atomic plane wave incident onto a diffraction grating of period d . The diffraction grating may be of either the amplitude or phase variety, where an amplitude (phase) grating spatially modulates the amplitude (phase) of the incident atomic wavefunction. In addition, the amplitude grating–atom interaction results in a reduction of the atomic flux, whereas the phase grating–atom interaction does not. Accordingly, the atomic wavefunction immediately after interacting with the grating is given by:

$$|\Psi\rangle = \sum_{n=-\infty}^{\infty} c_n |g, n\hbar k_{\text{g}}\rangle \quad (36)$$

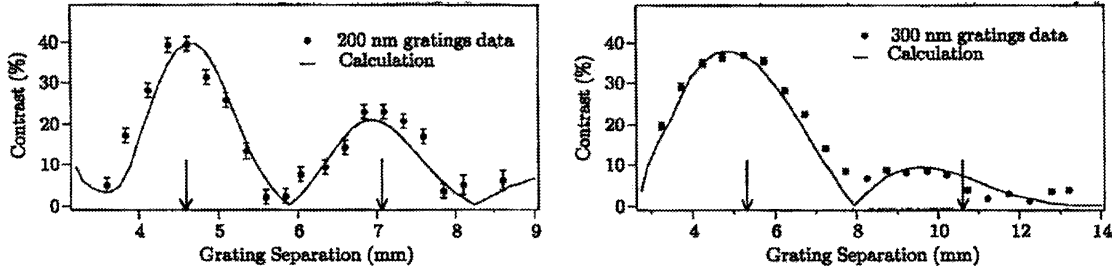


Figure 6. The matter-wave Talbot effect using amplitude diffraction gratings. Experimental data and calculations showing the contrast of the self-image as a function of grating separation. The first grating produces a diffraction pattern while the second grating acts as a read-out mask. Thus, as the second grating is scanned along the transverse direction, the total transmitted atom flux measured will display a fringe pattern with respect to the transverse position of the second grating. The measured contrast of these fringe patterns as a function of grating separation is a measure of the quality of the self-image formed by the first grating. The arrows indicate grating separations that are half integral multiples of the Talbot length, L_T . Figure from [18].

where $k_g = 2\pi/d$ is the grating wavevector and $|c_n|^2$ is the probability of the grating transferring $n\hbar k_g$ of transverse momentum to the atoms (assuming a normalized wavefunction). These momentum states are also energy eigenstates in free space and thus evolve in time according to a simple multiplicative phase factor:

$$|\Psi(t)\rangle = \sum_{n=-\infty}^{\infty} c_n |g, n\hbar k_g\rangle e^{-in^2 \hbar k_g^2 t / (2m)} \quad (37)$$

where m is the atomic mass and for convenience we have taken the end of the grating-atom interaction to be at $t = 0$. Thus we see that at later times the atomic wavefunction reproduces itself (to within a phase factor) whenever $t = n\tau_T$, $n = 1, 2, 3, \dots$, where the Talbot time, τ_T , is given by:

$$\tau_T = \frac{2md^2}{h} \quad (38)$$

For a standing light wave grating (equation (2)) $d = \lambda/2$. This renders the Talbot time:

$$\tau_T = \frac{\pi}{2\omega_{\text{rec}}} \quad (39)$$

The temporal atom optical Talbot effect using a standing wave light grating has been demonstrated by researchers at NIST [30]. They applied a pulsed standing wave to a BEC in the Kapitza-Dirac scattering regime. The self-focusing of the grating was measured with a second standing wave light grating pulse in analogy to the second grating described in figure 6 [18], and the Talbot time (39) derived above was verified experimentally.

In an atomic beam experiment, the Talbot length, L_T , is given by the product of the atomic longitudinal velocity, v , and the Talbot time, τ_T :

$$L_T = v\tau_T = \frac{2d^2}{\lambda_{\text{dB}}} \quad (40)$$

where $\lambda_{\text{dB}} = h/mv$ is the atomic de Broglie wavelength. An example of the Talbot effect in an atomic beam is shown in figure 6. The contrast of the replica grating whose period is the same as the original grating is shown as a function of downstream distance [18].

5. Summary of standing wave–atom interactions

The atomic motion induced by interaction with a standing light wave varies qualitatively as the interaction parameters used to study it are changed [31–36]. *Figure 7* summarizes the various interaction regimes of an atom with a standing wave in terms of the two most basic parameters: the two-photon Rabi frequency, $\omega_R^{(2)} = \omega_R^2/2\delta$, and the duration of the interaction, τ . To render the plot independent of atomic species, $\omega_R^{(2)}$ is given in units of the single-photon recoil frequency, ω_{rec} , and τ is given in units of the inverse single-photon recoil frequency, ω_{rec}^{-1} . Thus, for ^{23}Na the point (1,1) on *figure 7* corresponds to (6.4 μs , $2\pi \times 25$ kHz). The product of the two-photon Rabi frequency and the duration of the interaction is the pulse area, $\theta = \omega_R^{(2)}\tau$ (equation (31)), which is likewise the product of the pair of coordinates forming a point on the plot.

The lines KD1 and KD10 on *figure 7* show where the first maxima of $P_{1,10} = J_{1,10}^2(\theta)$ (equation (30)) occur, corresponding to the maximum possible population transfer into the first and tenth Kapitza–Dirac

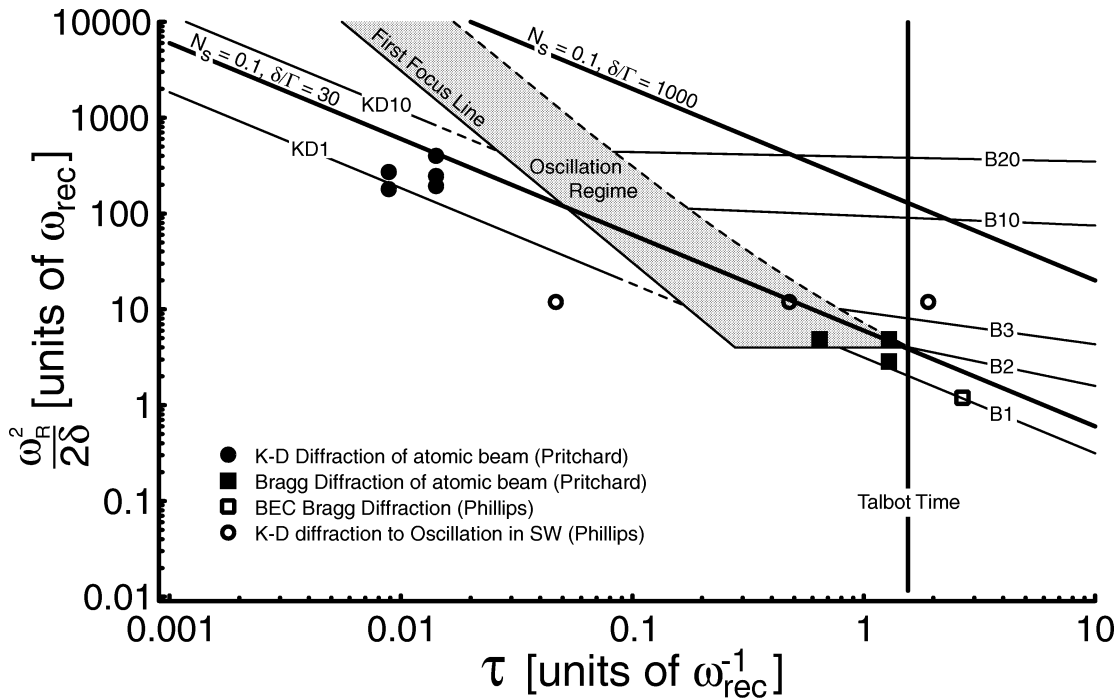


Figure 7. Atomic diffraction from a standing light wave (Section 5). The vertical axis is the two-photon Rabi frequency, $\omega_R^2/2\delta$, in units of the single-photon recoil frequency, ω_{rec} , and the horizontal axis is the pulse duration, τ , in units of the inverse single-photon recoil frequency, ω_{rec}^{-1} . The scaling is chosen to eliminate the atomic species dependence of the plot. All coherent momentum transfer processes are destroyed by spontaneous decay, which occurs with probability $N_s = 0.1$ along the lines labeled accordingly and parameterized by the given ratio δ/Γ . Lines KD1 and KD10 show conditions for the maximum transfer into the first and tenth Kapitza–Dirac diffracted order, respectively. As the interaction time is increased the Raman–Nath approximation is violated (termination of Kapitza–Dirac curves) and the atoms enter the oscillatory regime, executing at least a quarter period of oscillation above the *first focus* line (shaded area). Curves B1, B2, B3, B10, and B20 correspond to conditions that generate complete Bragg reflection in the first, second, third, tenth, and twentieth order, respectively. The thick vertical line shows the Talbot time, τ_T . Experimental conditions are shown as points. Filled circles: Kapitza–Dirac diffraction of an atomic beam [16]. Filled squares: Bragg diffraction of an atomic beam [7]. Open squares: Bragg diffraction of a BEC [15]. Open circles: transition from Kapitza–Dirac diffraction to oscillation of a BEC in a standing wave light pulse [17].

diffracted order respectively. Since the momentum distribution of diffracted atoms depends only on the pulse area, all Kapitza–Dirac orders are parallel to each other and further offset from the origin in increasing order number.

The Kapitza–Dirac regime ends at large interaction times where the Raman–Nath approximation fails due to motion of the atoms down the slope of the standing wave potential. We show these lines dashed as the interaction time approaches the beginning of the classical oscillation regime, and terminate these lines where the oscillation produces its first focus, at the *first focus* line. This line corresponds to the atoms completing a quarter period of oscillation in the standing wave potential, $\tau = \tau_{\text{osc}}/4$ (equation (34)).

In the shaded region of *figure 7*, the atoms will oscillate classically about the potential minimum, causing a periodic focusing of the atoms alternately in position and momentum space. However, anharmonicities of the potential away from its minimum will degrade the quality of the focusing effects.

The maximum diffracted order that can be significantly populated by the light–atom interaction is limited by energy conservation. Classically, the maximum momentum transfer to the atoms due to the sudden switch on of the standing wave is delivered to atoms that convert the full height of the standing wave potential ($\hbar\omega_{\text{R}}^2/\delta$), into kinetic energy. This gives:

$$\frac{p_{\text{max}}^2}{2m} \simeq \frac{\hbar\omega_{\text{R}}^2}{\delta} \implies p_{\text{max}} \simeq \omega_{\text{R}} \left(\frac{2\hbar m}{\delta} \right)^{1/2} \quad (41)$$

Equating the maximum absorbed momentum, p_{max} , to an integer number of two-photon recoil momenta yields the maximum expected diffracted order, N_{max} :

$$p_{\text{max}} = 2N_{\text{max}}\hbar k \implies N_{\text{max}} \simeq \frac{\omega_{\text{R}}}{2} (\omega_{\text{rec}}\delta)^{-1/2} \quad (42)$$

This is just half of the square-root of the standing wave potential height measured in units of the single-photon recoil energy:

$$N_{\text{max}} = \frac{1}{2} \left(\frac{\omega_{\text{R}}^2/\delta}{\omega_{\text{rec}}} \right)^{1/2} \quad (43)$$

As the two-photon Rabi frequency is reduced, N_{max} falls below unity. As a result, there is no longer time for the higher-order multi-photon processes to generate significant amplitudes in diffracted orders with $N > 1$ before dephasing due to the kinetic energy term (5) becomes significant and the higher order processes become negligible. Only a small population is ever transferred to the $N = \pm 1$ orders and it does not oscillate at ω_{rec} . Therefore the classical oscillation regime does not extend below $N_{\text{max}} \simeq 1$ where it is terminated on *figure 7*.

Classical oscillation would result in atoms with momentum from zero up to the maximum allowed by energy conservation. Therefore, the classical focusing of atoms must be manifest as an atomic population distribution over *many* of the quantized momentum states (separated by $2\hbar k$) allowed by energy conservation (equation (42)). However, as the interaction time lengthens and extends into the Bragg regime, the populated momentum states become restricted by energy conservation until only the oscillatory Pendellösung into and back from only one final state remains. Therefore, we have ended the classical oscillation regime where the Bragg condition (22) is satisfied. The Bragg regime presupposes a smooth light pulse shape. For a pulse with sharp edges, classically oscillatory behavior can still be observed at longer times than included in the shaded region of *figure 7*, which is why we show the large τ boundary of the classical oscillation regime as dashed.

In the Bragg regime, transfer of population is restricted to (and back from) only one final momentum state. The allowable final states are restricted by limiting the frequency bandwidth (i.e. energy uncertainty) of the light fields in the atomic rest frame. This is accomplished by lengthening the interaction time and

Table 1. Natural parameters and typical experimental parameters involved in standing wave diffraction. The relevant frequencies together with the corresponding times ($1/\omega$) are tabulated. The parameters for ^{23}Na have been used for system dependent quantities.

ω	ω_0	δ (Bragg)	ω_R (Bragg)	ω_R (K-D)	Γ	ω_{rec}	ω_{osc}
$\omega/2\pi$	500 THz	500 MHz	100 MHz	100 MHz	10 MHz	25 kHz	1 MHz
$1/\omega$	0.3 fs	0.3 ns	1.6 ns	1.6 ns	16 ns	6.4 μs	160 ns

smoothing the rise and fall of the electromagnetic fields. The parameters for a first order Bragg transition (table 1) are typically $\delta/\Gamma \simeq 50$, $\Gamma\tau \simeq 1$, and $\omega_R/\Gamma \simeq 10$ giving $N_s \simeq 10^{-2}$ and $\omega_R^{(2)}\tau \simeq 1$. Obtaining significant population transfer with higher-order Bragg processes requires larger intensities. Various orders (1, 2, 3, 10, and 20) of Bragg diffraction are shown as lines on figure 7 corresponding to $\omega_R^{(2N_B)}\tau = \pi$, where $\omega_R^{(2N_B)}$ is given in equation (21). The lines are terminated at the appropriate interaction time determined from the final momentum state resolution condition (22). The Bragg regime extends indefinitely to larger interaction times, which might be termed the region of Bragg spectroscopy. In experiments in this regime with ^{23}Na , atomic velocity resolution below 1 mm/s was obtained at $\tau = 80$ [8]. The study of adiabatically expanded BEC's would require larger interaction times to resolve their smaller velocity spread and weaker mean field shifts.

The Kapitza–Dirac and Bragg regimes assume a different initial atomic momentum (in the rest frame of the standing wave) parallel to the standing wave axis. Kapitza–Dirac scattering assumes no component of the initial atomic momentum along this axis. The efficiency of Kapitza–Dirac diffraction falls rapidly as the initial momentum in units of the photon momentum approaches $1/\omega_{\text{rec}}\tau$ [16]. To observe N_B -th-order Bragg scattering, the initial atomic momentum along the standing wave axis must have (non-zero) magnitude $N_B\hbar k$. Without adhering to this constraint, no final momentum state will be energetically degenerate with the initial state and the atomic sample will not respond to the presence of the standing wave, even if the interaction parameters are appropriate ($\omega_R^{(2N_B)}\tau \simeq 1$) for N_B -th-order Bragg scattering.

The condition $N_s = 0.1$ (equation (24)), where N_s is the expected number of spontaneous emission events per atom during the light–atom interaction, is drawn on figure 7 for two ratios (30 and 1000) of standing wave detuning, δ , to the atomic excited state natural lifetime, Γ . For fixed δ/Γ , we see that $N_s \propto \theta$, thus conditions with an increased pulse area (above and to the right of the $N_s = 0.1$ lines) result in a proportionally increased N_s . These $N_s = 0.1$ lines extend across all regimes of figure 7 because restricting spontaneous emission is required for both Kapitza–Dirac and Bragg scattering. As N_s approaches unity, the correct optical potential describing the light–atom interaction switches from equation (27) to equation (35). The atom lithography work mentioned in the text operated near the *first focus* line and an $N_s \simeq 1$ –3 line, a regime where equation (35) is valid.

It should be noted that scattering from standing waves in a regime where spontaneous emission is not negligible leads to new possibilities [37]. In the case of a two-level atomic system with the excited state coupled to a (third) dark state through a strong spontaneous decay channel, if the standing wave is tuned near resonance, the optical potential becomes complex valued due to the loss of atoms to the dark state. Furthermore, it becomes purely imaginary (absorptive or decohering) in the limit of zero detuning from resonance. Thus, while the standing wave fields in Section 3 behaved as phase gratings for an atomic sample, light gratings on resonance can effectively become amplitude diffraction gratings.

The thick vertical line in figure 7 is at the Talbot time, $\tau_T = \pi/2\omega_{\text{rec}}$ (equation (39)), and is 10 μs for ^{23}Na . It should be noted that to observe the Talbot effect, the atoms are exposed to two short pulsed standing wave fields separated temporally by the Talbot time. All other times on the plot denote the actual light–atom interaction time of a single interaction.

6. Conclusion

The manipulation of atoms using light forces from standing light waves is a rich subject. The seminal suggestion of Kapitza and Dirac laid dormant for 50 years due to lack of experimental technology. However, in the 1980s this suggestion was realized with atomic sources and considerably extended both experimentally and theoretically. In the early 1990s coherent standing wave manipulation became one of two major routes to making atom interferometers [7,16]. As the new century begins these techniques are being refined further with the replacement of thermal atomic beams by Bose-Einstein condensates (BECs) as atomic sources. In addition, stimulated light scattering techniques are forming the basis of new ways to study BECs, such as Bragg spectroscopy [8]. As progress continues, exciting developments should be forthcoming, such as definitive measurements of the fine structure constant, α , atom gyroscopes that are superior to the best laser gyroscope technology, and improved studies of BECs to further their applicability in the years ahead.

References

- [1] Pritchard D., Cronin A., Gupta S., Kokorowski D., Atom optics: old ideas, current technology, and new results, *Ann. Phys.* (2001), in print.
- [2] Kapitza P.L., Dirac P.A.M., The reflection of electrons from standing light waves, *Proc. Cambridge Philos. Soc.* 29 (1933) 297.
- [3] Pfeiffer H.C., *Phys. Lett.* 26 A (1967) 362.
- [4] Schwarz H., *Z. Phys.* 204 (1967) 276.
- [5] Roskos R., Bartell L., Thompson H., *Phys. Rev.* 166 (1968) 1494.
- [6] Takeda Y., Matsui I., *J. Phys. Soc. Jpn.* 25 (1968) 1202.
- [7] Martin P.J., Oldaker B.G., Miklich A.H., Pritchard D.E., Bragg scattering of atoms from a standing light-wave, *Phys. Rev. Lett.* 60 (1988) 515–518.
- [8] Stenger J., Inouye S., Chikkatur A.P., Stamper-Kurn D.M., Pritchard D.E., Ketterle W., Bragg spectroscopy of a Bose-Einstein condensate, *Phys. Rev. Lett.* 82 (1999) 4569–4573.
- [9] Aspect A., Arimondo E., Kaiser R., Vansteenkiste N., Cohen-Tannoudji C., *Phys. Rev. Lett.* 61 (1988) 826.
- [10] Aspect A., Arimondo E., Kaiser R., Vansteenkiste N., Cohen-Tannoudji C., *J. Opt. Soc. Am. B* 6 (1989) 2112.
- [11] Marte M., Stenholm S., *App. Phys. B* 54 (1992) 443.
- [12] Shull C.G., Observation of Pendellösung fringe structure in neutron diffraction, *Phys. Rev. Lett.* 21 (1968) 1585.
- [13] Ewald P., *Ann. Phys.* 54 (1917) 519.
- [14] Giltner D.M., McGowan R.W., Lee S.A., Theoretical and experimental study of the Bragg scattering of atoms from a standing light-wave, *Phys. Rev. A* 52 (1995) 3966–3972.
- [15] Kozuma M., Deng L., Hagley E.W., Wen J., Lutwak R., Helmerson K., Rolston S.L., Phillips W.D., Coherent splitting of Bose-Einstein condensed atoms with optically induced Bragg diffraction, *Phys. Rev. Lett.* 82 (1999) 871–875.
- [16] Gould P.L., Ruff G.A., Pritchard D.E., Diffraction of atoms by light — the near-resonant Kapitza-Dirac effect, *Phys. Rev. Lett.* 56 (1986) 827–830.
- [17] Ovchinnikov Y.B., Muller J.H., Doery M.R., Vredenburg E.J.D., Helmerson K., Rolston S.L., Phillips W.D., Diffraction of a released Bose-Einstein condensate by a pulsed standing light wave, *Phys. Rev. Lett.* 83 (1999) 284–287.
- [18] Chapman M., Ekstrom C., Hammond T., Schmiedmayer J., Tannian B., Wehinger S., Pritchard D., Near-field imaging of atom diffraction gratings: The atomic Talbot effect, *Phys. Rev. A* 51 (1995) R14–R17.
- [19] Timp G., Behringer R., Tennant D., Cunningham J., Prentiss M., Berggren K., Using light as a lens for submicron, neutral-atom lithography, *Phys. Rev. Lett.* 69 (1992) 1636–1639.
- [20] McGowan R.W., Giltner D.M., Lee S.A., *Opt. Lett.* 20 (1995) 2535.
- [21] McClelland J., Scholten R., Palm E., Celotta R., Laser-focused atomic deposition, *Science* 262 (1993) 877–880.
- [22] Gupta R., McClelland J., Jabbour Z., Celotta R., *App. Phys. Lett.* 67 (1995) 1378.
- [23] Gordon J., Askin A., Motion of atoms in a radiation trap, *Phys. Rev. A* 21 (1980) 1606.
- [24] Dalibard J., Cohen-Tannoudji C., *J. Opt. Soc. Am. B* 2 (1985) 1707.
- [25] Talbot H., *Philos. Mag.* 9 (1836) 401.
- [26] Flanders D., Hawryluk A., Smith H., Spatial-period-division — a new technique for exposing submicrometer-linewidth periodic and quasi-periodic patterns, *J. Vac. Sci. Technol.* 16 (1979) 1949.

BOSE-EINSTEIN CONDENSATES AND ATOM LASERS

Coherent manipulation of atoms

- [27] Hawryluk A., Smith H., Osgood R., Ehrlich D., Deep UV spatial period division using an excimer laser, *Opt. Lett.* 7 (1982) 402.
- [28] Hawryluk A., Smith H., Ehrlich D., Deep UV spatial-frequency doubling by combining multilayer mirrors with diffraction gratings, *J. Vac. Sci. Technol. B* 1 (1983) 1200.
- [29] Nowak S., Kurtsiefer C., Pfau T., David C., High-order Talbot fringes for atomic matter waves, *Opt. Lett.* 22 (1997) 1430.
- [30] Deng L., Hagley E., Denschlag, Simsarian J., Edwards M., Clark C., Helmerson K., Rolston S., Phillips W.J., Temporal, matter-wave-dispersion Talbot effect, *Phys. Rev. Lett.* 83 (1999) 5407–5411.
- [31] Special issue, *Prog. Quantum Electron.* 8 (1984).
- [32] Special issue, *J. Opt. Soc. Am. B* 2 (1985).
- [33] Special issue, *J. Opt. Soc. Am. B* 6 (1989).
- [34] Special issue, *App. Phys. B* 54 (1992).
- [35] Adams C., Sigel M., Mlynek J., *Phys. Rep.* 240 (1994) 143.
- [36] Special issue, *App. Phys. B* 60 (1995).
- [37] Oberthaler M., Abfalterer R., Bernert S., Schmiedmayer J., Zeilinger A., Atom waves in crystals of light, *Phys. Rev. Lett.* 77 (1996) 4980–4983.